Autofocus of Stripmap SAS Data using the Range-Variant SPGA Algorithm

H. J. Callow, M. P. Hayes, and P. T. Gough
Acoustics Research Group,

Dept. of Electrical and Computer Engineering,
University of Canterbury,
Private Bag 4800, Christchurch, NZ
{h.callow,m.hayes,p.gough}@elec.canterbury.ac.nz

***Abstract*— This paper presents an extension of the Stripmap Phase Gradient Autofocus (SPGA) algorithm to allow operation in environments where the grazing angle varies with range. SPGA is designed for stripmap autofocus in a low-grazing angle scenario. Autofocus performance is degraded when imagery that has varying grazing angles is autofocused using SPGA.**

The SPGA extension presented here models the combined effect of slant-plane towfish sway and heave on the data. This enhanced modelling allows the algorithm to operate in situations where the grazing angle to the scene varies with range.

Results from the application of the new algorithm to field-collected and simulated data sets are demonstrated. The range-variance SPGA extensions improve autofocus performance on simulation data that has varing grazing-angle. The field-collected dataset shown has little range variance and shows only minor improvement. We also present a short summary of simulation approximations giving consideration to quantitative autofocus testing.

I. Introduction

Synthetic Aperture Sonar (SAS) offers higher resolution at long range than conventional techniques. The increased resolution possible using SAS comes at the cost of increased processing and susceptibility to platform deviations. Increasing computing power has reduced the costs associated with SAS processing leaving platform deviation as the major concern.

Unknown platform deviations of sub-wavelength order lead to degradation of SAS imagery; this causes image blurring and poorer overall resolution. These problems can be ameliorated by either measuring the platform motion to within SAS motion constraints with an Inertial Navigation System (INS) or estimating the same motions with a data-driven autofocus technique. Once estimated the degrading effects of the platform deviations can be removed, restoring high-resolution imagery.

Autofocus techniques have proved successful in the radar analogue of SAS, Synthetic Aperture Radar (SAR). The most popular technique for SAR autofocus is Phase Gradient Autofocus (PGA) [1], [2]. The technique is restricted to spotlight imaging geometries rather than the strip-map modes common in SAS imaging.

The Strip-map Phase Gradient Autofocus (SPGA) algorithm has recently been developed to extend PGA to the geometries common in SAS imaging [3], [4]. SPGA was originally designed for low-grazing angle situations where sway effects every range identically; sway estimation and correction both rely on this assumption. When imaging a scene with a varying grazing-angle, the algorithm can underestimate the correction needed. The extension we describe in this paper is based on the Phase Weighted Estimation (PWE) proposed by Thompson *et. al* [5][1] and prevents underestimation in geometries with varying grazing angles (it also has the potential to estimate heave).

The notation of this paper follows that of [7].

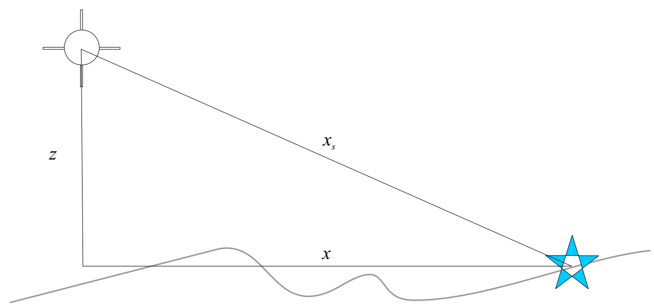

Fig. 1. Slant-range mapping. The across-track distance variable x and the height variable z are replaced by a single parameter x_s.

II. Slant-range geometry

The height dimension to the problem is considered in what is known as the slant-plane geometry [8]. Fig. 1 illustrates this transformation. The slant-range variable is x_s, which is given by the non-linear (polar) mapping

$$x_s = \sqrt{x^2 + z^2}, \tag{1}$$

$$\eta = \tan^{-1}\left(\frac{z}{x}\right), \tag{2}$$

where z is the sea-floor height and η is the grazing angle.

2-D image reconstruction techniques reconstruct the slant-plane image, $ff_s(x_s, y)$; i.e., the image coordinates are in x_s, y.

[1]The stripmap autofocus extension proposed in the same papers is similar to the mPGA algorithm [6] and we would expect SPGA to perform better in SAS imaging scenarios.

0-933957-31-9

Traditional autofocus routines have been derived for shallow water (ground-plane) situations where $\eta \approx 0$ and $x_s \approx x$; they assume that sway affects all ranges of the pulse-compressed image identically. As can be seen in Fig. 1, horizontal sway motions have little effect at close range and heave becomes more important. In situations with varying slant-angles (η) both range-variant motions compensation and phase estimation are required.

III. Range-variant motion compensation

When using efficient block processing reconstruction algorithms that process uniform linear array data, motion compensation is required as a preliminary step (to coerce data into uniform linear array form). Traditional ground-plane motion compensation based on the timing error approximation [4] corrects the pulse compressed data via

$$ss(u,t) \approx \widetilde{ss}\left(u, t + \frac{2X(u)}{c}\right), \tag{3}$$

where $\widetilde{ss}(u,t)$ is the distorted image, $ss(u,t)$ the ideal pulse-compressed image, and $X(u)$ the sway to be corrected. Often motion compensation is implemented in the Fourier domain.

In a slant-range situation the effect a sway has on a given target is a function of the slant-range depression angle η. This may be summarised for correction as

$$ss(u,t) \approx \widetilde{ss}\left(u, t + \frac{2X(u)\cos\eta}{c}\right), \tag{4}$$

$$\approx \widetilde{ss}\left(u, t + \frac{2X(u)x}{c\sqrt{x^2+z^2}}\right). \tag{5}$$

The narrow-beam approximation used in the timing error derivation

$$x \approx ct/2$$

may be used to calculate the correction as a function of the received time-delay

$$ss(u,t) \approx \widetilde{ss}\left(u, t + \frac{tX(u)}{\sqrt{(ct/2)^2+z^2}}\right). \tag{6}$$

Eq. (6) is a coordinate transform they may be implemented via a re-sampling operation.

Given Eq. (6) it is possible to compensate both sway and heave (sonar height that changes with along-track position $Z(u)$) under varying slant-angle within the constraints of the timing error approximation.

IV. Phase Weighted Estimation (PWE)

PWE as described by Thompson *et. al* [5] models the non-unique mapping between sway, heave, and slant-range phase error. This mapping is expressed as

$$\Delta r(u) = X(u)\cos\eta + Z(u)\sin\eta, \tag{7}$$

for a given slant-angle η where $\Delta r(u)$ is the slant-range shift at position u estimated from autofocus.

In an autofocus scenario there are many mappings each with a different slant-angle. When each mapping is written in matrix form the inversion becomes more apparent

$$\mathbf{A}_n\mathbf{M} = \mathbf{r}_n, \tag{8}$$

where

$$\mathbf{A}_n = [\cos\eta_n, \sin\eta_n],$$

$$\mathbf{M} = [X(u), Z(u)]^{\mathrm{T}},$$

and

$$\mathbf{r}_n = \Delta r_n(u).$$

Thus

$$\mathbf{M} = \mathbf{A}_n^{-1}\mathbf{r}_n, \tag{9}$$

where an SVD-based psuedo-inverse is used for $\mathbf{A}_n^{-1}$. The result $\mathbf{M}$ provides an estimate of $X(u)$ and $Z(u)$ to be used directly in motion-compensation. Note that the estimation is usually performed on phase gradients instead of distances, providing sway and heave phase gradients. This is because the traditional limitations of direct phase averaging also affect PWE.

The consequence is both heave and sway may be estimated given autofocus estimates from various slant-ranges (and angles). Sway underestimation caused by near-range (and steep slant-range) targets is avoided since the reduced effect of sway on the target is considered.

V. Range-variant SPGA algorithm

Range-variant SPGA is an extension of SPGA to allow the use of the phase weighted estimation outlined earlier. As such most of the algorithm is identical to that described in [4]. The range-variant SPGA algorithm operates as follows:

Step 1: Correct for known sway $X(u)$ using Eq. (6).

Step 2: Reconstruct image $\widetilde{ff}(x,y)$ from $\widetilde{ss}(u,t)$, say using the wavenumber algorithm.

Step 3: Find prominent points in $\widetilde{ff}(x,y)$ and associate coordinates (x_m, y_m). Note that x_m and y_m do not need to be found to sub-pixel precision.

Step 4: Create masks $W_m(x,y)$ centred on (x_m, y_m), where

$$W_m(x,y) = \mathrm{rect}\left(\frac{x-x_m}{W_x}\right)\mathrm{rect}\left(\frac{y-y_m}{W_y}\right). \tag{10}$$

Step 5: Form images containing regions of interest by multiplying $\widetilde{ff}(x,y)$ by the masks $W_m(x,y)$,

$$\widetilde{ff}_m(x,y) = \widetilde{ff}(x,y)W_m(x,y). \tag{11}$$

Step 6: 2-D Fourier transform $\widetilde{ff}_m(x,y)$ to $\widetilde{FF}_m(k_x,k_y)$.

Step 7: Determine the average along-track spatial energy density spectrum using

$$\beta_m(k_y) = \int_{-\infty}^{\infty} \left|\widetilde{FF}_m(k_x,k_y)\right|^2 dk_x. \tag{12}$$

Step 8: Calculate the centroid of the along-track spatial energy density spectrum allowing for circular wrapping using

$$\Delta k_{y_m} = \frac{k_{y\max}}{\pi} \text{phase} \left\{ \iint \left| \widetilde{f}_m(k_x, k_y) \right|^2 dk_x \times \exp\left(j \frac{\pi k_y}{k_{y\max}} \right) dk_y \right\}. \quad (13)$$

Step 9: Estimate the local linear sway gradient,

$$\sigma_m = \frac{\Delta k_{y_m}}{2k_0}. \quad (14)$$

Step 10: Estimate the true target position (x'_m, y'_m)

$$x'_m = x_m, \quad (15)$$
$$y'_m = y_m - \sigma_m x_m. \quad (16)$$

Step 11: Phase correct the spatial spectrum to account for the estimated target position

$$\widetilde{FF}'_m(k_x, k_y) = \widetilde{FF}_m(k_x, k_y) \exp\left(-jk_x(x'_m - x_m)\right) \exp\left(-jk_y(y'_m - y_m)\right). \quad (17)$$

Step 12: Apply wavenumber transform to form $\chi_m(k_x, u)$ from $\widetilde{FF}'_m(k_x, k_y)$,

$$\chi_m(k_x, u) = \widetilde{FF}'_m \left(k_x \frac{y_m - u}{x_m}, k_x \right). \quad (18)$$

Step 13: Calculate the complex error gradient using a sheared product

$$\psi_m(k_x, u) = \chi_m(k_x, u + \Delta u)\chi^*_m(k_x, u). \quad (19)$$

Step 14: Average the individual phase error gradients in frequency and assign each estimate to the vector $\mathbf{r}_m(u)$

$$\mathbf{r}_m(u) = \int_{-\infty}^{\infty} \psi_m(k_x, u) dk_x. \quad (20)$$

Step 15: Estimate z_m the sea-floor height for the coordinates x_m, y_m either by bathymetry or other prior knowledge.

Step 16: Calculate the slant-range mapping for each x_m, y_m and assign to the $\mathbf{A}_m$

$$\mathbf{A}_m = \left[\frac{x_m}{\sqrt{x_m^2 + z_m^2}}, \frac{z_m}{\sqrt{x_m^2 + z_m^2}} \right]. \quad (21)$$

Step 17: Calculate the heave and sway phase error gradient estimates via Eq. (9).

Step 18: Discard[2] the heave phase error gradient estimate and assign the sway phase gradient estimate to $\varphi(u)$.

Step 19: Integrate the phase error gradients

$$\varphi(u) = \varphi(y - \Delta u) + \Delta\varphi(y - \Delta u). \quad (22)$$

[2]Ideally this information should also be used for autofocus purposes.

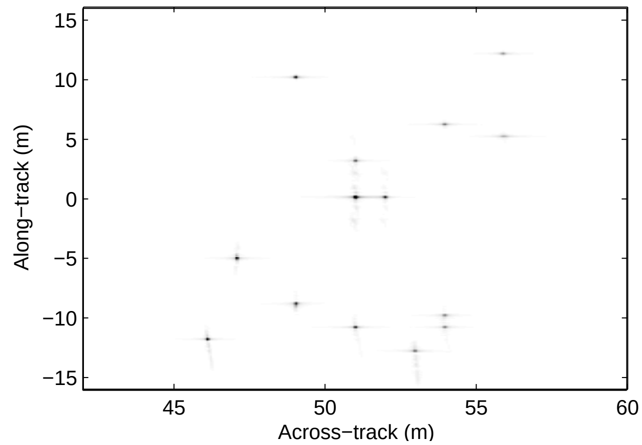

Fig. 2. Simulated target scene used in range-variant SPGA testing. The scene is 10 m below the sonar.

Step 20: Scale the phase error estimate by the wavelength of the centre frequency and estimate the residual sway

$$\hat{X}_i(u) = \frac{\varphi(u)}{2k_0}. \quad (23)$$

Step 21: Iterate algorithm until the residual sway is smaller than some threshold. The total estimated sway is the sum of the estimated residual sways from each iteration:

$$\hat{X}(u) = \sum_{i=1}^{I} \hat{X}_i(u). \quad (24)$$

VI. Results

A simulated SAS scene consisting of a 15 m by 30 m patch of point-scatters was used to test the proposed algorithm. The patch used is depicted in Fig. 2 and was located at 50 m in range and 10 m below the sonar. The sonar model used matches the kiwiSAS-II sonar (see [4]). The target scene, whilst small, does exhibit a changing grazing-angle and traditional SPGA underestimates the sway.

Fig. 3 shows the convergence of range-variant SPGA versus the original SPGA. The convergence is measured via the RMS sway gradient error as it maps well to image blurring [9]. Note that range-variant SPGA has improved performance when compared with baseline SPGA.

Further testing was performed on the field-data collected using the kiwiSAS-II in Sydney Harbour (the data-set is further described in [4]). Autofocus results are shown in Fig. 4: Fig. 4(a) shows the result of 2 iterations of unmodified SPGA and Fig. 4(b) the same using range-variant SPGA. The SPGA modifications have made only minor changes to autofocus performance on this scene. This is simply because the sonar is only a small distance above the sea-floor—approximately 2.5 m estimated from the first bottom bounce. Only the closest ranges in the scene have significantly varying grazing angle implying the small-grazing angle approximations inherent in SPGA are reasonable for this data. Some slight improvement

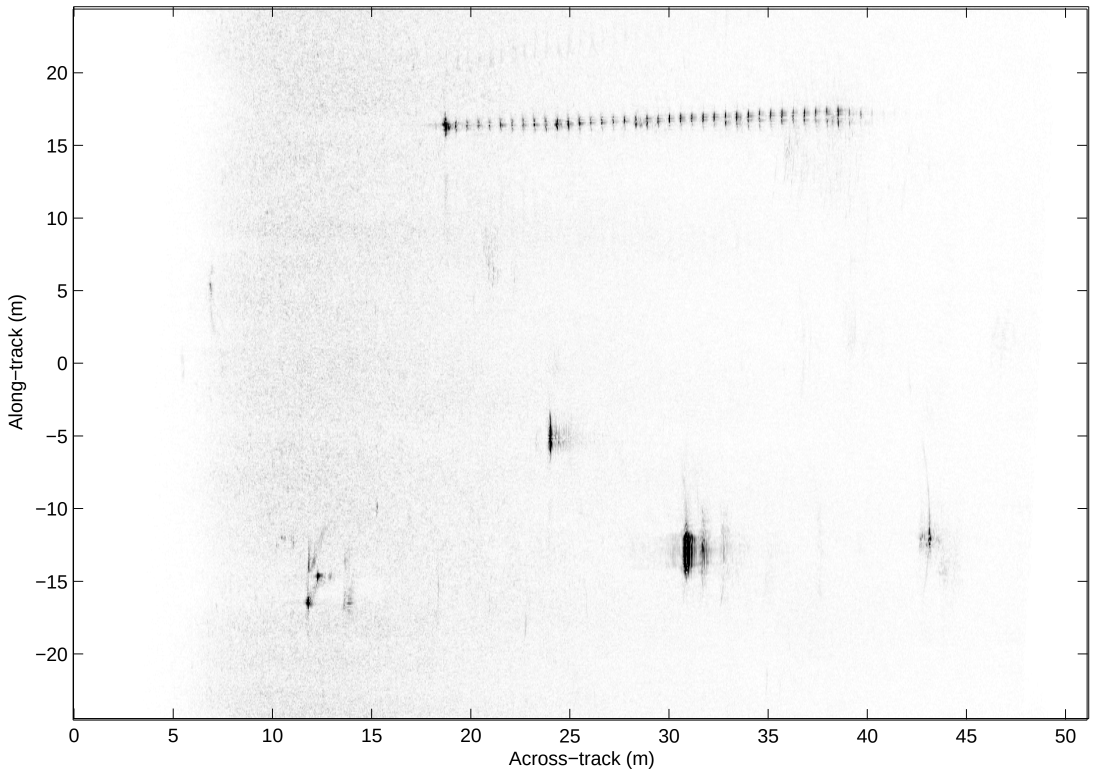

(a)

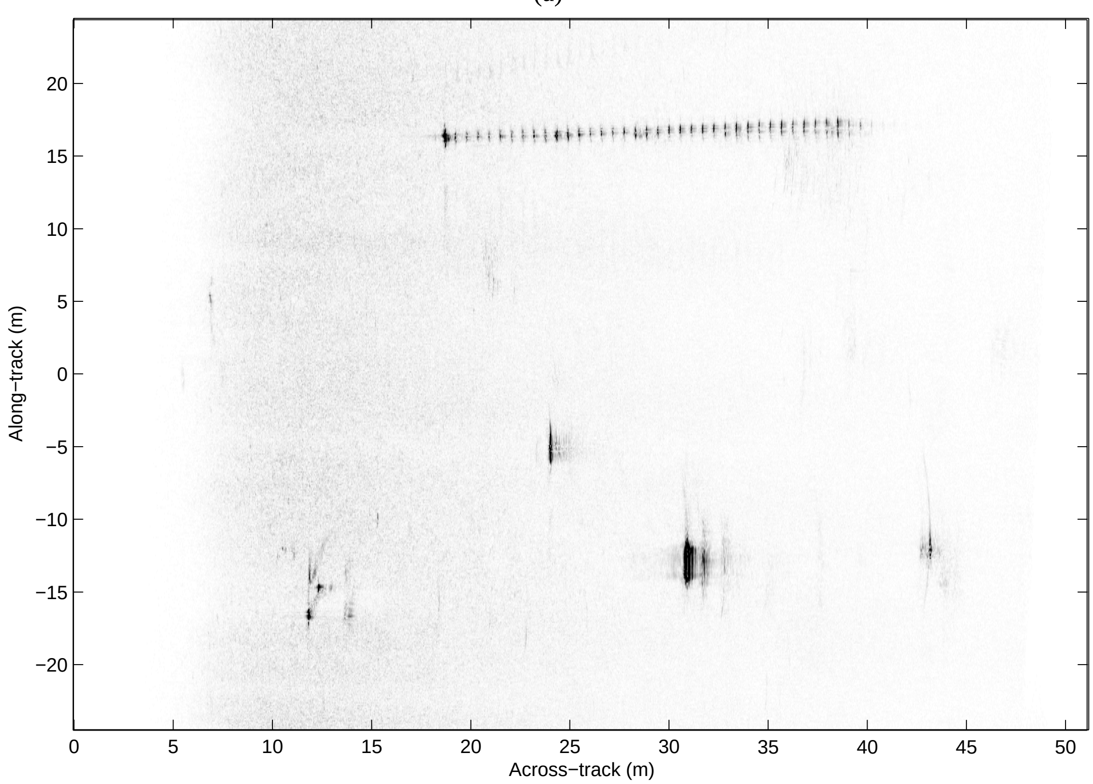

(b)

Fig. 4. Sydney Harbour data (a) reconstructed image with original SPGA autofocus (b) Range-variant SPGA autofocused image.

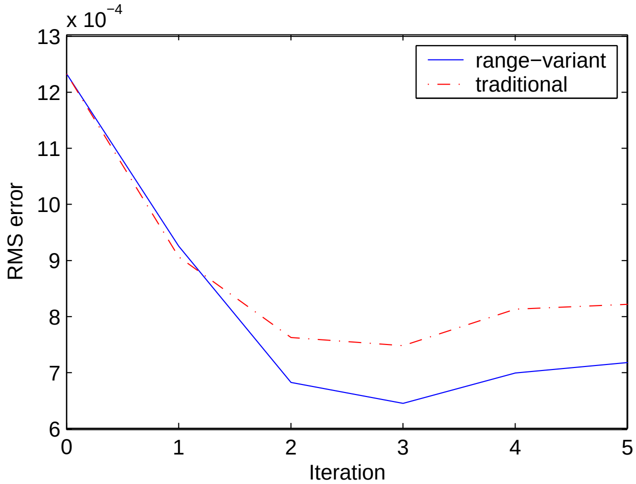

Fig. 3. Convergence rates of normal and range-variant SPGA.

in the focus of short-range targets is apparent on close inspection.

VII. Simulation Approximations and Autofocus

Autofocus performance must be considered carefully when using simulated data sets. Seemingly innocuous assumptions and approximations with regard to imagery can have large impacts on autofocus performance[3]. Testing with simulated clutter in particular needs to be clearly thought out as the spatial correlation lengths and amplitude probability density functions of clutter have effects on autofocus performance. Moreover, occlusion, shadowing, and non-Lambertian scattering have *significant* effects. Very few (if any) open simulation systems can accurately model frequency and position variant phase effects in shadow zones. These effects are common in field-collected data but currently rare in simulation for autofocus testing. A simulation suite is currently under development to address some of these issues [11].

VIII. Conclusions

We have proposed and demonstrated modifications to the SPGA autofocus algorithm to improve its performance in scenes with varying grazing angle. These improvements consist of an altered phase-estimation kernel based on PWE, improved modelling, and a new slant-range motion-compensation technique.

Preliminary results indicate that the modifications to allow for range-variance give improved autofocus. The improvement in autofocus is dependent on how much the grazing angle varies across the scene—shallow water scenes and scenes with only small variations derive limited benefit from using range-variant SPGA. In the field-collected data, which has little range-variance, only minor improvement was noted over baseline SPGA.

Future work will be concentrating on improving the weighted phase estimation with the aim of using higher-order phase estimators. Further testing on both simulated an field-collected data is required to show algorithm robustness.

[3]An example for PGA is given by Zavattero *et. al* [10]

Acknowledgments

We would like to acknowledge partial sponsorship of the work by the Department of the Navy, NAVSEA Coastal Systems Staion, Panama City, Florida, USA as grant N61331-00-G003 and grant N61331-02-C-0031.

References

[1] C. V. Jakowatz, Jnr., D. E. Wahl, P. H. Eichel, D. C Ghiglia, and P. A. Thompson, *Spotlight-Mode Synthetic Aperture Radar: A Signal Processing Approach*, Kluwer Academic Publishers, Boston, 1996.

[2] D. E. Wahl, P. H. Eichel, D. C. Ghiglia, and C. V. Jakowatz, Jnr., "Phase gradient autofocus – a robust tool for high resolution SAR phase correction," *IEEE Transactions on Aerospace and Electronic Systems*, vol. 30, no. 3, pp. 827–835, July 1994.

[3] M. P. Hayes, H. J. Callow, and P. T. Gough, "Strip-map phase gradient autofocus," in *Image and vision computing New Zealand 2002*, David Kenwright, Ed., Auckland, December 2002, pp. 71–76.

[4] H. J. Callow, M. P. Hayes, and P. T. Gough, "Stripmap phase gradient autofocus," To be presented at OCEANS 2003, 2003.

[5] D. G. Thompson, J. S. Bates, D. V. Arnold, and D. G. Long, "Extending the phase gradient autofocus alogrithm for low-altitude stripmap mode SAR," in *Proceeding of the Internation Geoscience and Remote Sensing Symposium 1999*, 1999, vol. 1, pp. 564–566.

[6] W. W. Bonifant, Jnr., "Interferometric synthetic aperture sonar processing," M.S. thesis, Georgia Institute of Technology, July 1999.

[7] P. T. Gough and D. W. Hawkins, "Imaging algorithms for a strip-map synthetic aperture sonar: Minimizing the effects of aperture errors and aperture undersampling," *IEEE Journal of Oceanic Engineering*, vol. 22, no. 1, pp. 27–39, Jan. 1997.

[8] M. Soumekh, "A system model and inversion for synthetic aperture radar imaging," *IEEE Transactions on Image Processing*, vol. 1, no. 1, pp. 64–76, Jan. 1992.

[9] H. J. Callow, "Signal processing for synthetic aperture sonar image enhancement," PhD. thesis (under examination), April 2003.

[10] Paul Zavattero, "Distributed target SAR image de-blurring using phase gradient autofocus," in *The record of the Radar Conference*. IEEE, 1999, pp. 246–249.

[11] A. J. Hunter, M. P. Hayes, and P. T. Gough, "Simulationm of wideband interferometric SAS imagery," in *OCEANS 2003*, 2003, To be presented.